# Amorphization in iron nitride thin films prepared by reactive ion-beam sputtering

Ranu Dubey,[1] Ajay Gupta,[1,*] and J. C. Pivin[2]
[1]*UGC-DAE Consortium for Scientific Research, University Campus, Khandwa Road, Indore 452017, India*
[2]*CSNSM-IN2P3, Bâtiment 108, 91405 Orsay Campus, France*

(Received 21 May 2006; revised manuscript received 15 September 2006; published 14 December 2006)

Reactive ion-beam sputtering has been used to prepare iron nitride over a wide composition range. It is found that the samples deposited at room temperature exhibit amorphous phase in the composition range from 12 at. % nitrogen to 23 at. % nitrogen. For samples deposited at liquid nitrogen temperature the system is amorphous up to 35 at. % nitrogen. Amorphization can be understood in terms of a frustration in the system due to a competition between $\alpha$ and $\varepsilon$ phases. Kinetic constraints are also found to play a role in the amorphization process. Mössbauer measurements suggest that the local order in the amorphous phase consists of a mixture of $\alpha$-Fe–like and $\varepsilon$-$Fe_3N$–like short-range orders. On the iron rich side the amorphous phase exhibits two-step crystallization, with a primary $\alpha$-Fe phase precipitating out in the first step. Around 22 at. % nitrogen the system exhibits a single step isomorphous transformation to $\varepsilon$ phase. Thus, amorphous iron nitride phases exhibit behavior very similar to the conventional transition metal-metalloid amorphous alloys. In the remaining composition range nanocrystalline phases are formed. The amorphous magnetic iron nitride phases are expected to have distinct advantages over their crystalline counterparts in terms of soft magnetic applications.

DOI: 10.1103/PhysRevB.74.214110 PACS number(s): 61.43.Dq, 64.70.Kb, 61.18.Fs, 68.55.−a

## I. INTRODUCTION

Amorphous alloys continue to attract significant attention in recent years. The issues related to the glass formation as well as atomic level structure in these systems are still not settled.[1–8] The main glass forming alloy families are (a) transition metal–metalloid systems, for example Fe-B and Fe-P, (b) early transition metal–late transition metal alloys like FeZr and FeTi, or (c) simple metallic glasses like MgZn. Recently discovered multicomponent systems which have exceptional stability with respect to crystallization, generally known as bulk metallic glasses, have renewed interest in this field. More recently, several binary systems like CaAl, CuZr, and CuHf have been identified which form glassy phase with high stability.[9–11]

Numerous studies have been devoted to the study of mechanism of glass formation. Several factors such as eutectic composition,[3,12–14] atomic size mismatch,[15] and large negative heat of mixing[13] have been attributed to the formation of amorphous phase. In metal-metal binary alloys like CuMg glass formation is favored by large negative heat of formation, nondirectionality of bonds, and a tendency to maximize packing fraction.[7] Kinetic factors also play an important role in determining glass forming ability. Turnbull proposed that ratio of the glass transition temperature $T_g$ to the liquidus temperature $T_l$ is an important parameter in determining glass forming ability;[16] the smaller the difference between liquidus temperature and glass transition temperature, the higher the glass forming ability. This criterion can also explain a high glass forming ability in transition metal–metalloid metallic glasses around compositions corresponding to deep eutectics. Lu *et al.* have recently proposed that the crystallization temperature of the system should also play an important role in determining glass forming ability, since glass formation is a competing process between liquid phase and the resulting crystalline phases;[1] if the liquid phase is stabilized upon cooling and competing crystalline phases are difficult to precipitate out, then glass formation would be facilitated.

In the present work, we report a detailed study of amorphous phase formation in an unusual glass forming system of Fe-N.[17,18] The Fe–N bonds are known to be one of the strongest covalent bonds and therefore the system can be considered as an extreme case of transition metal–metalloid metallic glasses. While the structure of metal-metal amorphous alloy can generally be described in terms of dense random packing of hard spheres because of the nondirectionality of the metallic bonding, transition metal–metalloid alloys possess covalent bonds, which are directional in nature, and therefore these alloys have rather well defined short range order.[19] Therefore, it would be interesting to study the short range order in an amorphous Fe-N system possessing strong covalent bond. A systematic study of metastable phase formation as a function of alloy composition provides some clue about the mechanism of amorphous phase formation in this system. It is found that amorphization in this system occurs due to a competition between two competing crystalline phases. Mössbauer spectroscopy has been used to get information about short-range order in the system.

Iron nitrides are also important because of their high hardness and excellent soft magnetic properties on the iron rich side.[20–22] An amorphous microstructure is expected to further improve the soft magnetic properties of iron nitride through the influence of amorphous microstructure on magnetic anisotropy, transport properties, etc.[23] Therefore, study of amorphous alloys of Fe-N is also interesting from an application point of view.

## II. EXPERIMENT

The iron nitride thin films of various compositions were deposited using reactive ion-beam sputtering on float glass

 

substrates.[24] The sample holder was mounted at a distance of 15 cm from the target. The base pressure during deposition in vacuum chamber was $1\times10^{-6}$ torr and the pressure during deposition was $4\times10^{-4}$ torr. The chamber was flushed with Ar several times in order to reduce the oxygen partial pressure, before putting on the ion source. In order to enrich the iron nitride sample with $^{57}$Fe, for Mössbauer measurement, the $^{57}$Fe foil of dimension $15\times30$ mm (purity 99.99%) was kept on the iron target. The target was sputtered by the ions of Ar and N (purity 99.995%) gas mixture. The accelerating voltage of 1000 V and the beam current of 25 mA was used during the deposition. The composition of the nitrogen in the sample was varied by varying the Ar to N gas ratio, keeping the total gas flow constant at 5 standard cubic centimeters per minute. Substrates were kept at room temperature during deposition. With increasing ratio of nitrogen in the flowing gas, the partial pressure of nitrogen in the chamber as well as the fraction of N ion in the beam will increase. Some of the films were also deposited with substrate kept at liquid nitrogen (LN2) temperature. It is expected that at lower temperature the mobility of the atoms at the surface would be lower, thus resulting in a more disordered and possibly amorphous phase. Different films are designated according to their corresponding nitrogen concentration, e.g., $S_L5$,$S_R12$, where 5 and 12 stand for the at. % of nitrogen present in the sample and subscripts $L$ and $R$ stand for the temperature of the substrate being at LN2 temperature and room temperature, respectively.

The composition of the films was determined using by Rutherford backscattering spectrometry (RBS) and nuclear reaction analysis (NRA). N, O, and C were dosed quantitatively by using the $^{14}N(d,p)^{15}N$, $^{16}O(d,p)^{17}O$, $^{12}C(d,p)^{13}C$ nuclear reaction with a deuteron beam of 1 MeV and a collection of the protons at an angle of 150° with respect to the incident beam. The energy of deuterons was chosen such that the cross section of each reaction remains reasonably constant over the depth range probed by the deuteron beam. The integral of $C(d,p0)$, $O(d,p1)$, $N(d\cdot p4+p5)$ peaks was normalized to that recorded from diamondlike pure C, pure silica, and pure $Si_3N_4$ films with thickness and density known from the RBS and ellipsometry measurement. Film thickness is estimated from RBS analysis and this technique permits us to determine concentration of Fe with accuracy better than 1%. The RBS analysis was performed with $He^+$ ions of relatively low energy (1 MeV) for improving the depth resolution, at normal incidence and with a collection of the scattered ions at an angle of 165°. Typical oxygen and carbon contamination (e.g., in sample $S_R15$) are 3 at. % and 2 at. %. This contamination is mainly superficial and appears high because of the low thickness of the film (50–100 nm). Therefore, the average oxygen contamination in the interior of the film is expected to be 1–2 at. % only.

The x-ray diffraction measurements were done using the Rigaku rotating anode x-ray generator in Bragg-Brentano geometry. $^{57}$Fe conversion electron Mössbauer spectroscopy measurements were done using the Wissel spectrometer in constant acceleration mode using a $^{57}$Co Rh source and a gas flow proportional counterdetector with a mixture of He +4% $CH_4$ gas. Crystallization behavior of the amorphous samples has been studied by annealing at various temperatures in a vacuum of $10^{-7}$ Torr.

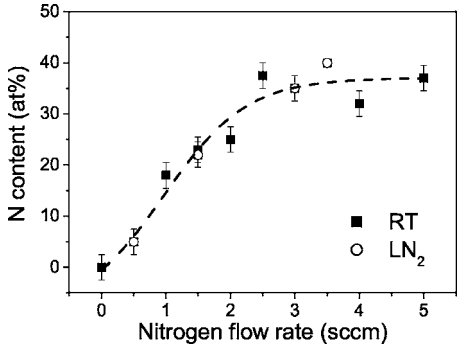


FIG. 1. Nitrogen concentration in the sample as a function of nitrogen flow rate for the samples deposited at room temperature and liquid nitrogen temperature. The error bar comes mainly from composition variation in the film.

## III. RESULTS AND DISCUSSION

### A. Amorphous phase formation

Figure 1 shows the average nitrogen content in the films as a function of the flow rate of nitrogen gas in the ion source for the sample deposited at both room temperature and liquid nitrogen temperatures. Nitrogen content was measured using RBS/NRA. However, in some cases analysis of the Mössbauer spectra was used to determine nitrogen content in the samples as discussed later. From RBS/NRA it was found that the composition of the films exhibits a variation of about 5% from point to point. The values reported are the average values taken over 10 points. As expected the nitrogen content in the film increases with increasing nitrogen flow rate, which results due to higher partial pressure of nitrogen in the chamber. However for sufficiently high nitrogen flow rate the nitrogen content in the film exhibits a saturation behavior. When pure nitrogen ions were used for sputtering, the maximum content of nitrogen in the film was found to be about 40 at. %. There is no significant difference in the nitrogen content in the films deposited at room temperature and those deposited at liquid nitrogen temperature. This behavior is in contrast to that observed in some earlier studies where iron nitride films were deposited by reactive magnetron sputtering:[25] It was found that films deposited at 523 K had a lower nitrogen content because of some desorption of nitrogen at that temperature. In the present case, since at room temperature desorption of nitrogen is expected to be negligible, there is no difference between nitrogen content in the film deposited at room temperature and liquid nitrogen temperature.

Figure 2 gives an x-ray diffraction (XRD) pattern of the as-deposited films. One may note that for the films deposited at room temperature, with nitrogen content ranging between 12 and 23 at. %, XRD spectra exhibits only a broad hump around $2\theta\sim41°$–$43°$, indicating that these films are amorphous in nature. In the case of films deposited at liquid nitrogen temperature, the range of amorphization extends up to 35 at. % nitrogen. Film with 5 at. % nitrogen shows a rela-

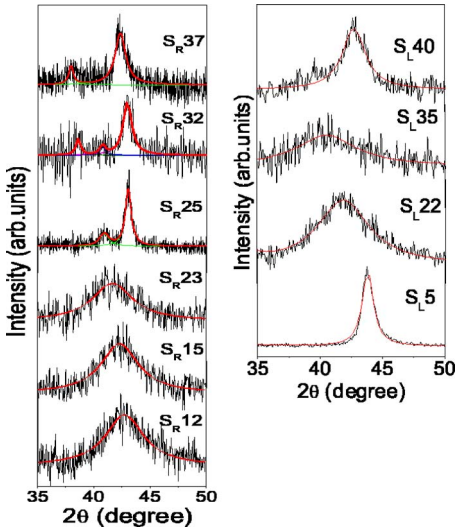


FIG. 2. (Color online) XRD patterns of the pristine samples deposited at (a) room temperature and (b) liquid nitrogen temperature with various nitrogen concentration.

tively sharp crystalline peak around $2\theta=43.8°$ which corresponds to a (110) peak of Fe, indicating that it is primarily an $\alpha$-Fe phase with some nitrogen dissolved in it. For films deposited at room temperature, when nitrogen content becomes $>23$ at. % the films again exhibit relatively sharp diffraction peaks indicating their crystalline nature. The diffraction peaks in specimen $S_R25$ correspond to the $\varepsilon$ phase having hexagonal structure, whereas specimens $S_R32$ and $S_R37$ may contain some admixture of a $\zeta$ phase or it may be a nonstoichiometric $\varepsilon$ phase. The crystallite size in all the cases is in the nanometer range.

The average near neighbor distance in case of amorphous films has been calculated using the relation

$$d = 1.23\lambda/2 \sin \theta.$$

It may be noted that the near-neighbor distance as calculated from XRD essentially gives the average distance between two Fe atoms, the scattering cross section for nitrogen atoms being significantly smaller. With increasing nitrogen concentration, the average Fe-Fe distance should increase. In the first approximation, the Fe-Fe distance can be written in terms of the Fe concentration $C_{\mathrm{Fe}}$ as

$$d_{\text{Fe-Fe}} \propto 1/C_{\mathrm{Fe}}^{1/3}.$$

Figure 3 shows a plot of average Fe-Fe distance deduced from the position of the XRD hump as a function of $1/C_{\mathrm{Fe}}^{1/3}$. As expected it exhibits an almost linear dependence.

Figure 4 gives the Mössbauer spectra of the films. On the iron rich side the films are magnetic in nature while for nitrogen content greater than 23 at. % the films become nonmagnetic. This is in conformity with numerous earlier studies on the FeN system. Further it may be noted that the films, which exhibit a broad hump in the XRD pattern, also exhibit a broad distribution of hyperfine field, which is again typical for amorphous phases. Mössbauer spectra of $S_R32$ and $S_R37$ consist of two overlapping doublets with hyperfine parameter of isomer shift (IS)=0.312 mm/s and quadrupole splitting

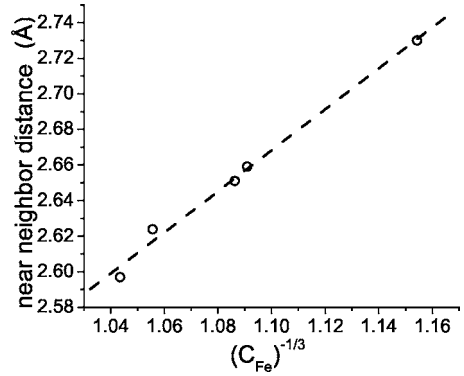


FIG. 3. Plot of average Fe-Fe distance as a function of Fe concentration.

(QS)=0.449 mm/s corresponding to first doublet, and IS=0.431 mm/s and QS=0.275 mm/s corresponding to second doublet. The values of the Mössbauer fitted parameter match with those of nonstoichiometric $\varepsilon$-$Fe_2N$. The relative areas of the two doublets have been used to get the nitrogen content.[20] The specimen $S_R25$ consists of a mixture of a broad magnetic component and a broad doublet indicating some composition inhomogenity in the system. Therefore, it was not possible to get reliable information about the structure and composition of the sample from the Mössbauer measurement. Mössbauer spectrum of specimen

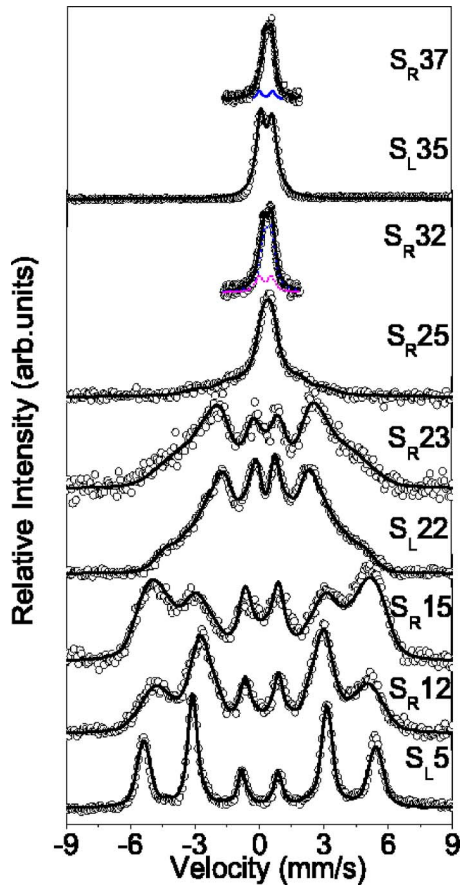


FIG. 4. (Color online) Some representative room temperature Mössbauer spectra as a function of nitrogen concentration.

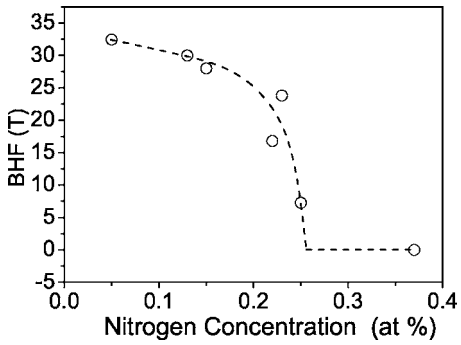


FIG. 5. Magnetic hyperfine values of the as-deposited samples at room temperature in pristine state.

$S_L35$, which is found to be amorphous from XRD measurements, consists of a single broad doublet and its hyperfine parameters (IS=0.32 mm/s; QS=0.55 mm/s) do not match with those of any known crystalline phases. The Mössbauer spectrum of the $S_L5$ consists of a single sextet with a hyperfine field of 32.5 T, confirming that it is $\alpha$-Fe with some nitrogen dissolved in it.

Figure 5 gives the average hyperfine field at room temperature in the films as a function of nitrogen content. One may note that initially the hyperfine field decreases slowly with nitrogen content and between 23 and 25 at. % nitrogen it rapidly drops down to zero. This dependence of hyperfine field on nitrogen content is similar to that observed in several iron nitrides prepared by various methods.[20,26] It may be pointed out that in earlier studies a rapid drop in hyperfine field is observed in the concentration range 29–32 at. %. Thus in the present case the system became nonmagnetic at N content about 6–7 at. % lower than the earlier cases. This difference may be attributed to a higher degree of disorder in the present system.

The above studies show that reactive ion-beam sputtering at room temperature results in formation of amorphous iron nitride phases in the composition range 12 at. % nitrogen to 23 at. % nitrogen. Outside this composition range on both sides the nanocrystalline phases are formed. This behavior can be understood in terms of the free energy diagram of Fe-N system, which is shown in Fig. 6, as taken from Ref. 27. One may note that in the composition range in which amorphous phase formation is observed in the present case, both $\alpha$ and $\varepsilon$ phases have comparable free energies. A very high degree of disorder which is expected in both $\alpha$ and $\varepsilon$ phases during deposition would further increase their free energies making thermodynamic distinction between the two phases more obscure. Thus, during deposition, the two phases would be competing with each other. This would result in some sort of frustration in the system, which would inhibit the development of long-range order, thus resulting in the formation of amorphous phase. This conjecture is also supported by the observed hyperfine field distribution in the amorphous samples (Fig. 7). One may note that the field distribution of the samples exhibits mainly two broad humps around 32 and 23 T covering the field of both $\alpha$-Fe(N) and $\varepsilon$ phases (marked by vertical lines). With increasing nitrogen content, the area under the hump around 23 T increases at the expense of the other, thus supporting the conjecture that

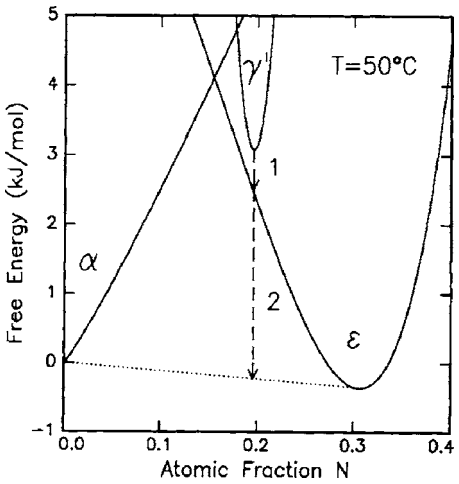


FIG. 6. Gibbs free energy of $\alpha$, $\varepsilon$, and $\gamma$ phase of iron nitride as a function of nitrogen concentration, as taken from Ref. 27.

the system contains both $\alpha$-Fe as well as $\varepsilon$-$Fe_3N$ types of short-range orders and that with increasing nitrogen content the fraction of $Fe_3N$ type short-range order increases.

An increase in the composition range over which amorphization is observed at low temperature indicates that kinetic constraints also play a role in the amorphization. At lower temperature the mobility of the atoms decreases, thus making atomic rearrangement in the films more sluggish, which inhibits the formation of long-range order.

Several criteria have been proposed in the literature for understanding the glass forming ability of various systems. The more acceptable criteria is that of the reduced glass transition temperature $T_{rg}=T_g/T_l$ introduced by Turnbull.[16] More recently Lu *et al.* have argued that glass formation is a competing process between a liquid phase and resulting crystalline phases.[1] Therefore, they have proposed a normalized crystallization temperature, defined as

$$\gamma = T_x[1/\{2(T_g + T_l)\}],$$

as a parameter to gauge the glass forming ability, where term $T_x$ is the absolute crystallization temperature. A good correlation is obtained between the parameter $\gamma$ and the glass

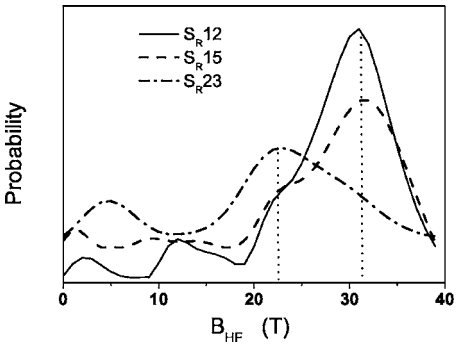


FIG. 7. Hyperfine field distribution in amorphous Fe-N samples as obtained from fitting of the conversion electron Mössbauer spectra.

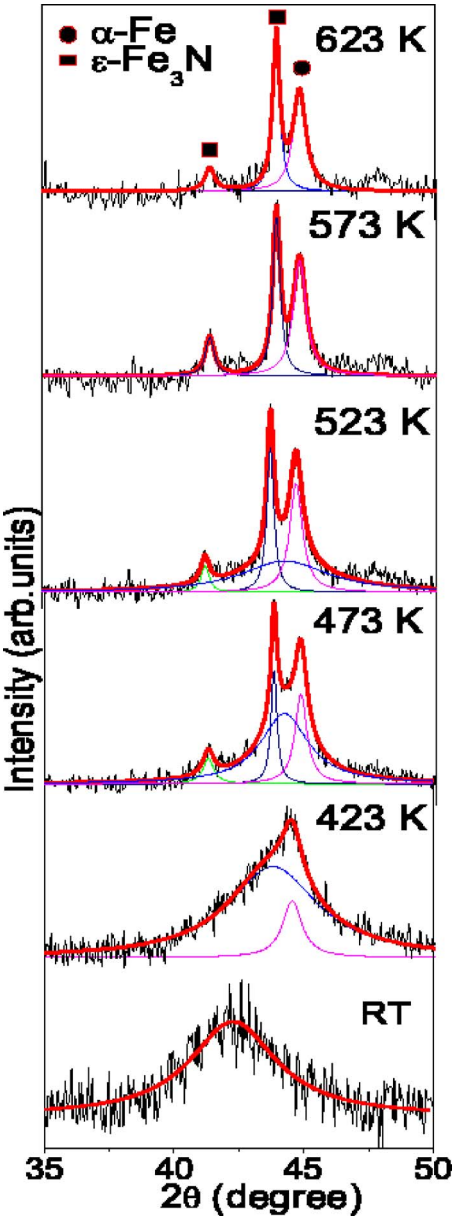


FIG. 8. (Color online) XRD pattern of sample $S_R15$ as a function of isochronal annealing at various temperatures.

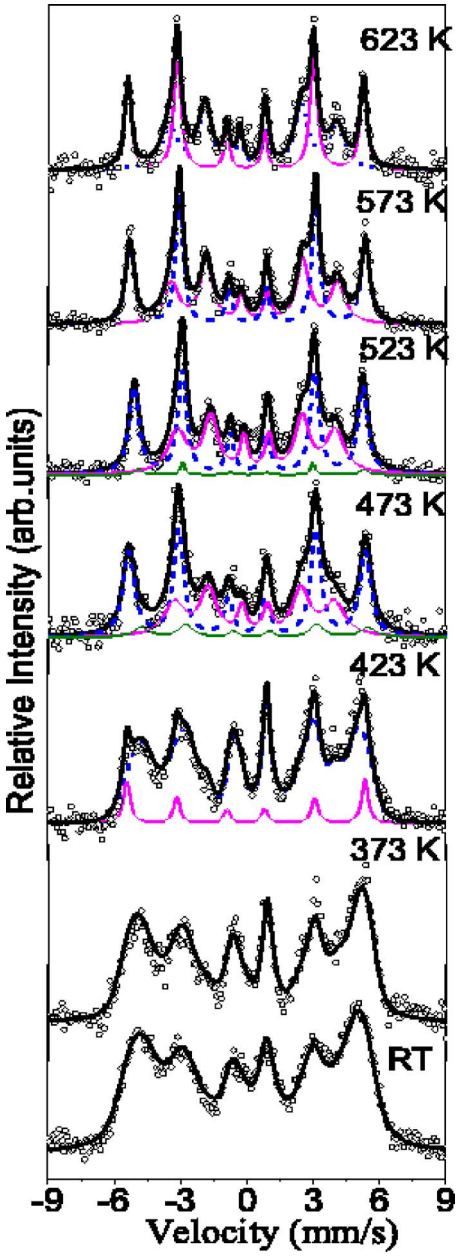


FIG. 9. (Color online) Conversion electron Mössbauer spectra of sample $S_R15$ as a function of isochronal annealing at various temperatures.

forming ability for a large number of metallic as well as oxide glasses. In contrast to this, in the present work we find that, in Fe-N system, a competition between two crystalline phases is the cause of amorphous phase formation.

It may be noted that in the context of the ease of glass formation around deep eutectic, it has been argued that around eutectic there are multiple ordered phases competing with each other and the crystallization of the liquid requires simultaneous rearrangement of different species of atoms, which significantly limits the kinetics of the process and thus promotes glass formation.[3,14] It may be noted that in the Fe-N phase diagram there also exists a eutectic at a composition of 12 at. % N, and therefore the observed amorphization in the system occurs preferentially around this eutectic composition.

### B. Annealing behavior of films

Detailed crystallization behavior of amorphous films $S_R15$ has been done. Figure 8 gives the XRD pattern of $S_R15$ as a function of isochronal annealing temperature. Figure 9 gives the corresponding Mössbauer spectra. Even at a temperature of 423 K the sample exhibits crystallization as evidenced from the appearance of an additional peak in the XRD pattern around $2\theta \approx 44.6°$, which corresponds to the (110) peak of $\alpha$-Fe. With increasing annealing temperature this peak grows in intensity, at the same time an additional peak in the XRD pattern around $2\theta \approx 43.8°$ appears indicating the formation of the $\varepsilon$ phase. With further annealing both $\alpha$ and $\varepsilon$ phases grow in intensity at the expense of the amorphous

TABLE I. The results of fitting of Mössbauer spectra of sample $S_R15$ as a function of annealing temperature.

| Annealing temp. (K) | Amorphous phase | | $\alpha$ phase | | $\varepsilon$ phase | |
|---|---|---|---|---|---|---|
| | $H$ (T) | Area (%) | $H$ (T) | Area (%) | $H$ (T) | Area (%) |
| RT | 28.2±0.1 | 100 | | | | |
| 373 | 28.5±0.1 | 100 | | | | |
| 423 | 26.8±0.1 | 90±5 | 33.3±0.1 | 10±5 | | |
| 473 | 31.8±0.1 | 9±5 | 33.2±0.1 | 53±5 | 22.4±0.1 | 38±5 |
| 523 | 31.5±0.1 | 3±5 | 32.1±0.1 | 51±5 | 22.1±0.1 | 46±5 |
| 573 | | | 33.0±0.1 | 53±5 | 23.3±0.1 | 47±5 |
| 623 | | | 33.0±0.1 | 51.0±5 | 23.4±0.1 | 49±5 |

phase; at the same time the crystallite size of both phases increases. In the Mössbauer spectrum also a distinct hyperfine field component around 33 T starts appearing at 423 K, which is typical of the $\alpha$-Fe phase. Mössbauer spectra of the samples annealed at a temperature of 423 K and above have been fitted with three overlapping sextets corresponding to $\alpha$ phase, $\varepsilon$ phase, and the remaining amorphous phase. The Mössbauer spectrum of this sample annealed at 473 K and above exhibits two relatively sharp hyperfine field components corresponding to 33 and 23 T. The hyperfine field and isomer shift of the second component correspond to the stoichiometric $\varepsilon$-$Fe_3N$ phase.[26] The results are given in Table I. From Table I the following conclusions can be drawn.

(1) In conformity with XRD results at 423 K only the $\alpha$-Fe phase precipitates out. In the range of 473 to 523 K all three phases, namely $\alpha$, $\varepsilon$, and the remaining amorphous phase are present. At 573 K the film is completely crystallized.

(2) After annealing at 473 K the hyperfine field of the $\varepsilon$ phase is 22.4 T, which is substantially lower than the hyperfine field of the stoichiometric $\varepsilon$-$Fe_3N$ phase (24.6 T). This suggests that the $\varepsilon$ phase, which precipitates out after annealing at 423 K, has higher N content. With increasing annealing temperature the hyperfine field of the $\varepsilon$ phase increase indicates some nitrogen loss.

These Mössbauer results are in conformity with the XRD measurement. Upon further annealing at higher temperature up to 623 K no new phase appears.

These studies show that the amorphous $S_R15$ specimen follows two-step crystallization. In the first step $\alpha$-Fe precipitates out while in the second step the remaining amorphous phase crystallizes into $\varepsilon$-$Fe_3N$. Thus this sample follows a typical crystallization behavior of hypereutectic amorphous alloys in which during the first crystallization step the primary metallic phase precipitates out with enrichment of amorphous phase in metalloid, while in the second step the remaining amorphous phase transforms into an isomorphous crystalline phase.[28] The first crystallization step starts around 423 K, while the second crystallization step is already partially completed after annealing at 473 K. Thus the two crystallization steps are rather overlapping. This may be partly due to the fact that there is some composition inhomogeneity in the sample that would result in a distribution of crystallization temperature, thus smearing out the crystallization steps.

After complete crystallization of the system the relative areas of the $\alpha$-Fe and $\varepsilon$-$Fe_3N$ phases are 53% and 47%, respectively. From this one can estimate the overall composition of the parent amorphous phase using the relation

$$C_N = A_1 C_{N1} + A_2 C_{N2},$$

where subscripts 1 and 2 represent the $\alpha$ and $\varepsilon$ phases present in the sample. The nitrogen content in the sample comes out to be 15 at. %.

Crystallization behavior of $S_R12$ is similar to that of $S_R15$. In this case also the two crystallization components are $\alpha$-Fe and stoichiometric $\varepsilon$-$Fe_3N$. However, as expected, in this case after complete crystallization at 573 K,[23] the amount of $\alpha$-Fe is more. The composition of the film as determined from the relative areas of the two subcomponents is 12 at. % nitrogen.

Figure 10 gives the XRD pattern of the specimen $S_R23$ as a function of isochronal annealing. Figure 11 gives the corresponding Mössbauer spectra. The XRD pattern after annealing at 423 K exhibits a sharp peak at $2\theta$ equal to 43.7° corresponding to the (101) reflection of $\varepsilon$-$Fe_3N$. In the Mössbauer spectrum after 423 K annealing the hyperfine field does not change significantly and only a small sharpening of the field distribution is observed. The average hyperfine field of the annealed samples is 23.8 T, which corresponds to the nonstoichiometric $\varepsilon$-$Fe_3N$ phase. The combined results of XRD and Mössbauer measurements present a picture in which around 423 K the amorphous phase isomorphously transforms into $\varepsilon$-$Fe_3N$. Thus, for lower nitrogen concentration, the amorphous phase crystallizes via a two step process while around 23 at. % nitrogen content the transformation is isomorphous. This behavior is similar to that observed in numerous metal-metalloid amorphous alloys.[28]

Thermal annealing of specimen $S_R25$ has also been studied. XRD data evidences only grain growth with increasing annealing temperature. In the Mössbauer spectrum, the pristine sample exhibits a small magnetic component, which disappears after annealing at 473 K. This small magnetic component in the pristine sample may be attributed to small composition inhomogenity as also evidenced by NRA/RBS measurements. Due to composition fluctuation, some region of the specimen may have Curie temperature above room temperature, thus giving rise to a magnetic component. An-

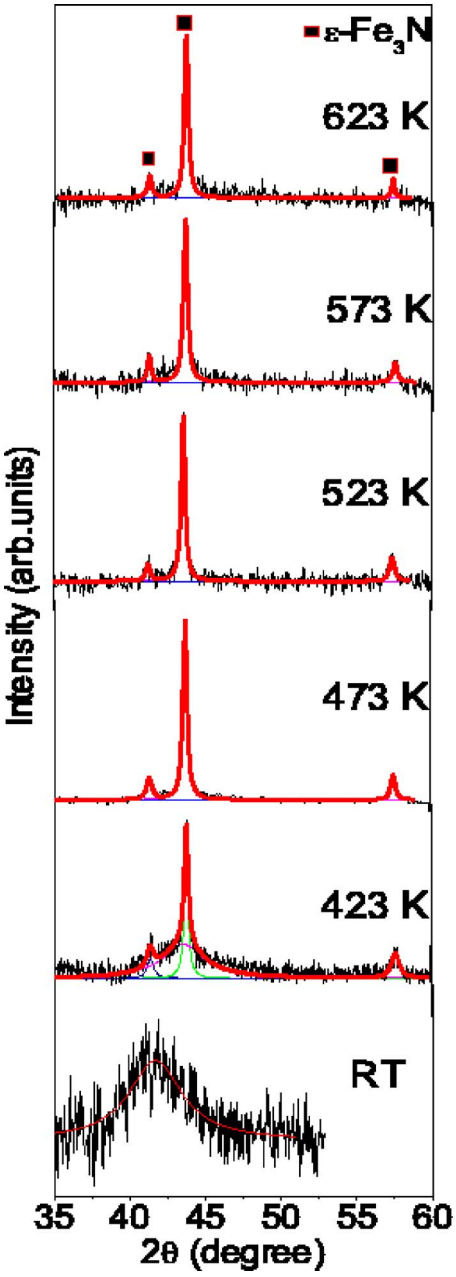


FIG. 10. (Color online) XRD patterns of sample $S_R23$ as a function of isochronal annealing at various temperatures.

nealing at 473 K results in homogenization of the sample due to increased mobility of nitrogen atoms, resulting in disappearance of the magnetic components.

## IV. CONCLUSIONS

Iron nitride phases over a wide composition range have been prepared using ion-beam sputtering. At room temperature the formation of the amorphous phase is observed in the composition range of 12 to 23 at. % nitrogen. On both sides of this range nanocrystalline phases are formed. Amorphization in this composition range is a result of a competition between $\alpha$-Fe and $\varepsilon$-$Fe_3N$ types of short-range orders. Deposition at $LN_2$ temperature results in a significant increase in the range of composition over which amorphization occurs. This suggests that the kinetic constraints also play an important role in the formation of the amorphous phase. Structure of the amorphous phase consists of a mixture of $\alpha$-Fe and $\varepsilon$-$Fe_3N$ type of short range orders, the relative abundance of which varies with the nitrogen content in the sample. The amorphous FeN system exhibits a crystallization behavior typical of metal-metalloid systems. On the Fe rich side the system exhibits two-step crystallization. In the first step a primary $\alpha$-Fe phase precipitates out, whereas in the second step the remaining amorphous phase transforms into $\varepsilon$-$Fe_3N$. The amorphous alloy with composition close to $Fe_3N$ isomorphously transforms into the $\varepsilon$ phase in a single step.

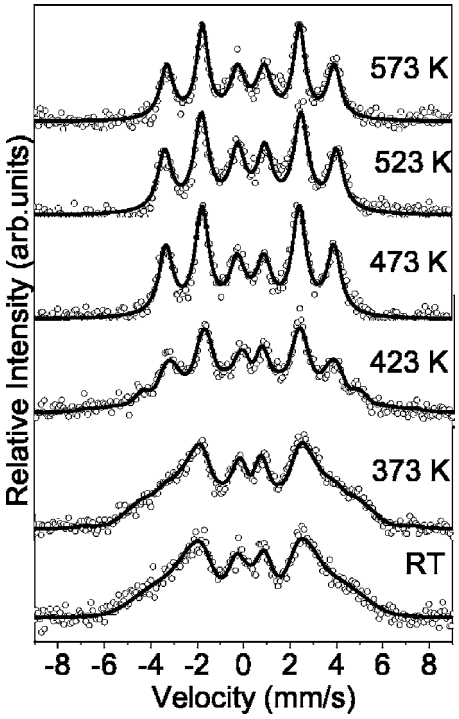


FIG. 11. Conversion electron Mössbauer spectra of sample $S_R23$ as a function of isochronal annealing at various temperatures.

## ACKNOWLEDGMENTS

Thanks are due to Satish Potdar for help in the deposition of thin films and to Joseph Salomon and Laurent Pichon of C2RMF France for their help in NRA analysis. Financial assistance from the Indo-French Center for Promotion of Advanced Research is acknowledged.

*Author to whom correspondence should be addressed. Email address: agupta@csr.ernet.in

[1] Z. P. Lu and C. T. Liu, Phys. Rev. Lett. **91**, 115505 (2003).
[2] S. Mukherjee, J. Schroers, W. L. Johnson, and W. K. Rhim, Phys. Rev. Lett. **94**, 245501 (2005).
[3] Donghua Xu, Gang Duan, and William L. Johnson, Phys. Rev. Lett. **92**, 245504 (2004).
[4] G. Duan, D. Xu, Q. Zhang, G. Zhang, T. Cagin, W. L. Johnson, and William A. Goddard III, Phys. Rev. B **71**, 224208 (2005).
[5] Nicholas P. Bailey, Jakob Schiøtz, and Karsten W. Jacobsen, Phys. Rev. B **69**, 144205 (2004).
[6] T. Ichitsubo, E. Matsubara, T. Yamamoto, H. S. Chen, N. Nishiyama, J. Saida, and K. Anazawa, Phys. Rev. Lett. **95**, 245501 (2005).
[7] Kyungsoo Ahn, Despina Louca, S. J. Poon, and G. J. Shiflet, Phys. Rev. B **70**, 224103 (2004).
[8] J. C. de Lima, D. Raoux, J. M. Tonnerre, D. Udron, K. D. Machado, T. A. Grandi, C. E. M. de Campos, and T. I. Morrison, Phys. Rev. B **67**, 094210 (2003).
[9] F. Q. Guo, S. J. Poon, and G. J. Shiflet, Appl. Phys. Lett. **84**, 37 (2004).
[10] D. Wang, Y. Li, B. B. Sun, M. L. Sui, K. Lu, and E. Ma, Appl. Phys. Lett. **84**, 4029 (2004).
[11] D. H. Xu, B. Lohwongwatana, G. Duan, W. L. Johnson, and C. Garland, Acta Mater. **52**, 2621 (2004).
[12] W. L. Johnson, JOM **54**(3), 40 (2002).
[13] A. Inoue, Acta Mater. **48**, 279 (2000).
[14] W. L. Johnson, Mater. Sci. Forum **225**, 35 (1996).
[15] D. B. Miracle, W. S. Sanders, and O. N. Senkov, Philos. Mag. **83**, 2409 (2003).
[16] D. Turnbull, Contemp. Phys. **10**, 473 (1969).
[17] M. Gupta, A. Gupta, J. Stahn, M. Horisberger, T. Gutberlet, and P. Allenspach, Phys. Rev. B **70**, 184206 (2004).
[18] Rachana Gupta and Mukul Gupta, Phys. Rev. B **72**, 024202 (2005).
[19] F. H. Sanchez, Y. D. Zhang, and J. I. Budnick, Phys. Rev. B **38**, 8508 (1988); I. Vincze, T. Kemeny, and Sigurds Arajs, *ibid.* **21**, 937 (1980).
[20] Peter Schaff, Prog. Mater. Sci. **47**, 1 (2002).
[21] Hiroshi Naganuma, Ryoichi Nakatani, Yasushi Endo, Yoshio Kawamura, and Masahiko Yamamoto, Sci. Technol. Adv. Mater. **5**, 101 (2004).
[22] H. Y. Wang, S. Mitani, M. Motokawa, and H. Fujimori, J. Appl. Phys. **93**, 9145 (2003).
[23] Ranu Dubey and Ajay Gupta, J. Appl. Phys. **98**, 083903 (2005).
[24] Mukul Gupta, Ajay Gupta, D. M. Phase, S. M. Chaudhari, and B. A. Dasannacharya, Appl. Surf. Sci. **205**, 309 (2003).
[25] Xin Wang, Weitao Zheng, and Lijuan Gao, Mater. Chem. Phys. **82**, 254 (2003).
[26] Peter Schaff, Hyperfine Interact. **111**, 113 (1998).
[27] L. de Wit, T. Weber, J. S. Custer, and F. W. Saris, Phys. Rev. Lett. **72**, 3835 (1994).
[28] U. Koster and U. Herold, in *Glassy Metals -I*, edited by H.-J. Guntherodt and H. Beck (Springer-Verlag, Berlin, 1981), p. 225.